Magnetic Resonance in Medicine 69:675–681 (2013)

Test–Retest Reproducibility of a Rapid Method to Measure Brain Oxygen Metabolism

Peiying Liu, Feng Xu, and Hanzhang Lu*

Cerebral metabolic rate of oxygen ($CMRO_2$) is an important index of tissue viability and brain function, but this parameter cannot yet be measured routinely on clinical scanners. Recently, a noninvasive technique was proposed which estimates global $CMRO_2$ by concomitantly measuring oxygen-extraction-fraction using T_2-relaxation-under-spin-tagging MRI and pulse oximetry, and cerebral-blood-flow using phase-contrast MRI. This study sought to establish a standard acquisition procedure for this technique and to evaluate its test–retest reproducibility in healthy subjects. Each subject was examined in five sessions and each session included two measurements. Intrasession, intersession, and intersubject coefficients of variation for $CMRO_2$ were found to be 3.84 ± 1.44% (N = 7, mean ± standard deviation), 6.59 ± 1.56%, and 8.80% respectively. These reproducibility values were comparable or slightly superior to ^{15}O positron emission tomography (PET) results reported in the literature. It was also found that oxygen-extraction-fraction and cerebral-blood-flow tended to covary across sessions (P = 0.002) and subjects (P = 0.01), and their coefficients of variation were greater than that of $CMRO_2$. The simplicity and reliability features may afford this global $CMRO_2$ technique great potential for immediate clinical applications. **Magn Reson Med 69:675–681, 2013. © 2012 Wiley Periodicals, Inc.**

Key words: cerebral metabolic rate of oxygen; cerebral blood flow; venous oxygenation; oxygen extraction fraction

Cerebral metabolic rate of oxygen ($CMRO_2$) refers to the amount of oxygen consumed by the brain per unit time, and is often written in units of mL O_2 per 100 g tissue per minute. Because oxidative metabolism is the primary means of energy production in the brain (1), $CMRO_2$ is an important index of tissue viability and brain health. Abnormal levels of $CMRO_2$ have been reported in a number of conditions such as Alzheimer's disease (2,3), brain aging (4), multiple sclerosis (5,6), Parkinson's disease (7), diabetes (8,9), traumatic brain injury (10), and normal pressure hydrocephalus (11). Therefore, a noninvasive, fast, and reliable method to quantify $CMRO_2$ is expected to have immediate impact in many clinical conditions.

Currently established methods for $CMRO_2$ measurement usually require the use of exogenous tracer (e.g., $^{15}O_2$ in positron emission tomography (PET) (12–15), $^{17}O_2$ in NMR (16), N_2O in Kety-Schmidt method (17,18), and ^{13}C in NMR (19)), continuous blood sampling, and special equipment (e.g., cyclotron). These complexities in experimental procedures in combination with the relatively high costs have prohibited $CMRO_2$ from becoming a routine clinical measure. More recently, a number of newer technologies have been proposed for the measurement of $CMRO_2$ without using exogenous tracers (20–32). Calibrated functional MRI (fMRI) uses purely vascular challenges to obtain an estimation of $CMRO_2$ percentage change associated with neural activation (24–27) and, when multiple physiologic challenges (e.g., hypercapnia and hyperoxia) are applied concomitantly, absolute $CMRO_2$ values may also be calculated (28). Other methods have used extravascular blood oxygen level-dependent (BOLD) effect (29), phase angle of venous blood (30), and optical properties of venous blood (31,32) to estimate $CMRO_2$.

Our laboratory has recently devised an MR method to estimate whole-brain $CMRO_2$ by combining noninvasive measurements of cerebral blood flow (CBF), arterial and venous oxygenation (21). In this method, whole brain CBF was measured by phase-contrast (PC) MRI (33) whereas arterial oxygenation (Y_a) was measured by pulse oximetry. The most challenging component, venous oxygenation (Y_v), was measured by a T_2-relaxation-under-spin-tagging (TRUST) MRI technique that was developed in our laboratory (34). Global $CMRO_2$ is calculated from these parameters using the Fick principle of arteriovenous difference (17). Despite the lack of spatial information, several desirable features of this method, e.g., noninvasiveness (no exogenous agent), fast (about 3–7 min in scan time), availability on a standard clinical scanner, allowed an easy application of the technique in several physiologic and clinical studies (4,5,35–37). These preliminary evidences demonstrated a great potential for this measure to serve as a biomarker in several neurological conditions. However, in order for this method to be widely used by the clinical community, a standard acquisition procedure as well as the test–retest reproducibility needs to be established.

Therefore, the purpose of this study is to describe a standard protocol for noninvasive evaluation of $CMRO_2$ and to test the reliability of this method. While Xu et al. (21) have shown a proof-of-principle of this design, the proposed protocol incorporated the more recent advances in the TRUST technique which allowed us to reduce the scan duration by 63% while maintaining measurement accuracy (38). The PC measurement has also been adjusted to better reflect global CBF. We studied seven healthy subjects and each subject was examined for five

Advanced Imaging Research Center, University of Texas Southwestern Medical Center, Dallas, Texas, USA.

Grant sponsor: NIH; Grant numbers: R01 MH084021, R01 NS067015, R21 AG034318, R01 AG033106.

*Correspondence to: Hanzhang Lu, Ph.D., Advanced Imaging Research Center, UT Southwestern Medical Center, 5323 Harry Hines Blvd., Dallas, TX 75390. E-mail: hanzhang.lu@utsouthwestern.edu

Received 3 February 2012; accepted 23 March 2012.

DOI 10.1002/mrm.24295

Published online 19 April 2012 in Wiley Online Library (wileyonlinelibrary.com).

times on different days. Within each session, the scans were repeated once. These data allowed us to evaluate the intrasession and intersession reproducibility as well as intersubject variations of CBF, Y_v, oxygen-extraction-fraction (OEF), and $CMRO_2$ measurements.

METHODS

Framework of the $CMRO_2$ Measurement

The theoretical basis of our $CMRO_2$ measurement is the Fick Principle of arteriovenous oxygen difference, a principle used by Kety and Schmidt in their original $CMRO_2$ measurement (17). Brain oxygen metabolic rate is given by:

$$CMRO_2 = CBF \cdot (Y_a - Y_v) \cdot C_a \quad [1]$$

where CBF is the whole-brain blood flow in mL/100 g/min, Y_a and Y_v are oxygen saturation fraction in arterial and venous blood in %, respectively; and C_a is the amount of oxygen molecules that a unit volume of blood can carry and is well established in physiology literature (897 μmol O_2/100 mL blood for hematocrit level of 0.44) (39). Some researchers further define a term called OEF, given by $OEF = (Y_a - Y_v)/Y_a \times 100\%$.

Y_v is determined using a recently developed and validated TRUST MRI technique (34,40). Briefly, TRUST MRI utilizes the spin-tagging principle on the venous side to separate out the pure venous blood signal by subtracting the labeled image from the control image. The label and control scans are performed with various numbers of flow-insensitive T_2-preparation pulses to modulate the signal with different T_2 weightings. The monoexponential fitting of the blood signal to the T_2-preparation duration (termed effective echo time [eTE]) then gives the T_2 value of the venous blood. As blood T_2 has a well-known relationship with the oxygenation level of the blood, the estimated venous T_2 can be converted to Y_v via a calibration plot obtained by a set of in vitro experiments (40).

Global CBF is measured by a PC quantitative flow technique (33) applied at the feeding arteries at the base of the brain. PC MRI utilizes the phase of an image to encode the velocity of moving spins and has been validated for angiogram and quantitative flow measurements (41–43).

Y_a is relatively homogenous across individuals. One can use literature values (e.g., 98%) or can measure this parameter noninvasively on the finger tip with pulse oximetry.

Sequence	Duration (min)	Purpose
Angiogram	1.4	PC positioning
TRUST MRI	1.2	Y_v measurement
PC on left ICA	0.5	CBF Measurement
PC on right ICA	0.5	CBF Measurement
PC on left VA	0.5	CBF Measurement
PC on right VA	0.5	CBF Measurement

FIG. 1. Proposed MRI procedure for a complete $CMRO_2$ dataset.

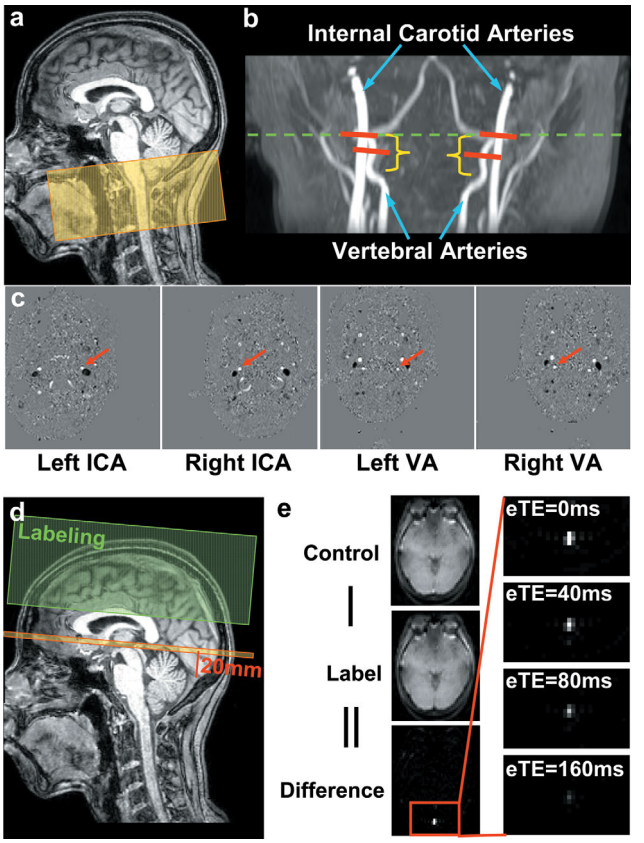

FIG. 2. Illustration of the positions of the MRI scans and representative images. **a**: Slice position of the 3D angiogram scan that is needed to visualize the feeding arteries. **b**: Typical results of the angiogram scan with slice positions of the PC MRI scans. The four PC MRI scans (red bars) are positioned perpendicular to the respective feeding arteries based on the maximum intensity projection image of the angiogram. The green dash line indicates the level of foramen magnum where the arteries enter the skull. The corresponding phase images from the PC MRI scans are shown in (**c**). The targeted arteries are pointed out by the red arrows. **d**: Imaging slice (yellow) and labeling slab (green) of the TRUST MRI scan. The imaging slice was positioned to be parallel to anterior-commissure posterior-commissure line with a distance of 20 mm from the sinus congruence. **e**: Typical data of TRUST MRI. The subtraction of the control and labeled images yields blood signal, which is then subject to increasing T_2 weightings. Monoexponential fitting of the signal as a function of eTE results in T_2 estimation.

Proposed Protocol for $CMRO_2$ Measurement

In this section, we provide detailed steps to obtain a complete $CMRO_2$ dataset, so that readers can feasibly reproduce these procedures (Fig. 1).

The measurement started with an axial 3D time-of-flight angiogram for which the top of the slab is at the level of the bottom of pons (Fig. 2a). This allowed the operator to visualize the feeding arteries of the brain which is necessary for PC MRI slice positioning (Fig. 2b). The imaging parameters of the time-of-flight angiogram were time of repetition (TR)/TE/flip angle = 20 ms/3.45 ms/18°, field of view (FoV) = 160 × 160 × 70.5

mm^3, voxel size = 1.0 × 1.0 × 1.5 mm^3, number of slices = 47, one 60-mm saturation slab positioned above the imaging slab, scan duration = 1.4 min.

After time-of-flight angiogram, a TRUST scan was performed. The imaging slice was positioned to be parallel to anterior-commissure posterior-commissure line with a distance of 20 mm from the sinus congruence where the superior sagittal sinus, straight sinus, and transverse sinus join (Fig. 2d). This empirical criterion allowed the imaging slice to intersect superior sagittal sinus at an angle close to 90°. A postsat TRUST sequence (38) was used with the following parameters: TR = 3000 ms, TI = 1200 ms, voxel size = 3.44 × 3.44 × 5 mm^3, four different T_2 weightings with eTEs of 0, 40, 80, and 160 ms, with a t_{CPMG} = 10 ms, scan duration = 1.2 min. The labeling slab was 100 mm in thickness and was positioned 22.5 mm above the imaging slice. This allows sufficient labeling of venous blood in upstream vessels.

While the TRUST scan was being performed, the operator planned the PC MRI scans. Based on the maximum intensity projection images from the time-of-flight angiogram, four PC MRI scans were planned corresponding to the four feeding arteries of the brain, left internal carotid artery, right internal carotid artery, left vertebral artery (left VA) and right vertebral artery (right VA), respectively (Fig. 2b). Ideally, the PC MRI slices should be placed at the level of foramen magnum where the arteries enter the skull (green dashed line in Fig. 2b). This was feasible for internal carotid arteries which do not make obvious turns in this region. For VAs, however, this was found to be difficult in practice due to complexity in vascular trajectory at this level. Therefore, the positions for VA PC MRI were chosen to be the mid point of an immediately lower segment (parentheses in Fig. 2b) of the arteries, which are slightly below foramen magnum. More discussions on the positioning of PC MRI and comparison to the previous study (21) are given in Discussion section. For all PC MRI scans, the center of the FOV was placed to overlap with the center of the targeted artery. This procedure allowed an easy identification of the proper artery during postprocessing, which is useful in practice as there are a considerable number of blood vessels in the neck region. Imaging parameters of PC MRI are: single slice, voxel size = 0.45 × 0.45 × 5 mm^3, FOV = 230 × 230 × 5 mm^3, maximum velocity encoding = 80 cm/s, 4 averages, scan duration of one PC MRI scan is 0.5 min.

The total duration to obtain a $CMRO_2$ dataset is ~ 5 min.

Reproducibility Study

Seven healthy subjects (three males, four females, age 26.4 ± 4.0 years) participated in the study. All MRI experiments were performed on a 3-T MRI scanner (Achieva, Philips Medical Systems, The Netherlands) using a body coil for radio frequency (RF) transmission and an eight-channel sensitivity encoding head coil for receiving. Foam padding was used to stabilize the head and minimize motion. The protocol was approved by University of Texas Southwestern Medical Center's Institutional Review Board and informed written consent was obtained from each participant.

Each subject was scanned on five separate sessions within a 13 day period, with a minimum gap of 1 day. During each session, the above-described $CMRO_2$ procedure was performed twice with a 12 min gap but without repositioning of the subject. In addition, a T_1-weighted magnetization-prepared rapid gradient-echo image (voxel size = 1 × 1 × 1 mm^3) was acquired in the first session of each subject to provide an estimation of the brain volume, so that variances in brain sizes can be accounted for when comparing $CMRO_2$ across subjects. Note that an anatomic scan is acquired in virtually all studies, thus this scan time was not included when calculating the time needed to obtain a $CMRO_2$ dataset. The arterial oxygen saturation fraction (Y_a, in %) was also measured once only (with a pulse oximetry device made by Invivo, Gainesville, FL) because Y_a is known to be relatively stable and its influence on $CMRO_2$ is expected to be small compared to the other experimental measures (4).

Data Analysis

Data processing of TRUST and PC MRI followed methods used previously (21,34,40). Briefly, for TRUST MRI data, after motion correction and pairwise subtraction between control and labeled images, a preliminary region-of-interest (ROI) was manually drawn to include the superior sagittal sinus. To further define the venous voxels, four voxels with the highest signals in the difference images in the ROI were chosen as the final mask for spatial averaging. The venous blood signals were then fitted to a monoexponential function to obtain T_2. The T_2 was in turn converted to Y_v via a calibration plot obtained by in vitro bovine blood experiments under controlled oxygenation, temperature, and Hct conditions (40). For PC MRI data, a ROI was manually drawn on the targeted artery of each PC MRI scans based on the magnitude image. The operator was instructed to trace the boundary of the targeted artery without including adjacent vessels. The phase signals, i.e., velocity values, within the mask were summed to yield the blood flow of each artery. To account for brain size differences, the unit volume CBF (in mL/100 g/min) was obtained by normalizing the total CBF (in mL/min) of all four arteries to the intracranial mass (in gram), which was estimated from the high resolution T_1-weighted magnetization-prepared rapid gradient-echo image using the software FSL (FMRIB Software Library, Oxford University). OEF was calculated from Y_a and Y_v.

Several reproducibility indices were calculated for each of the physiologic parameters evaluated. Intrasession coefficient of variation (CoV) was calculated as:

$$\mathrm{CoV}_{\mathrm{intrasession}} = \frac{1}{I.J}\sum_i\sum_j \frac{|M_{ij1} - M_{ij2}|}{\sqrt{2}\cdot \mathrm{Mean}(M_{ij1}, M_{ij2})} \quad [2]$$

where M_{ij1} and M_{ij2} represent measurement #1 and #2, respectively of Subject #i (i = 1, 2, ···, I) in Session #j (j = 1, 2, ···, J). Intersession CoV was calculated as:

$$\mathrm{CoV}_{\mathrm{intersession}} = \frac{1}{I.K}\sum_i\sum_k \frac{SD_j(M_{ijk})}{\mathrm{Mean}_j(M_{ijk})} \quad [3]$$

where SD stands for standard deviation.

Table 1
Summary of the Intrasession, Intersession, and Intersubject CoV (Mean ± SD, $N = 7$)

	Y_v	OEF	CBF	$CMRO_2$
Mean ± SD	61.73 ± 4.62 (%)	37.50 ± 4.83 (%)	60.57 ± 9.70 (mL/100 g/min)	182.25 ± 11.97 (μmol/100 g/min)
Intrasession CoV (%)	1.88 ± 0.57	3.19 ± 1.20	2.77 ± 0.82	3.84 ± 1.44
Intersession CoV (%)	5.06 ± 3.12	8.16 ± 4.46	7.41 ± 2.99	6.59 ± 1.56
Intersubject CoV (%)	9.15	15.61	17.40	8.80

Intersubject CoV was calculated as:

$$\mathrm{CoV}_{\mathrm{intersubject}} = \frac{1}{I.K}\sum_i \sum_k \frac{SD_i(M_{ijk})}{\mathrm{Mean}_i(M_{ijk})} \quad [4]$$

Compared to intrasession CoV, the value of intersession is expected to contain additional variance due to subject repositioning and day-to-day differences in physiologic states. These contributions can be calculated as $\sqrt{\mathrm{CoV}^2_{\mathrm{intersession}} - \mathrm{CoV}^2_{\mathrm{intrasession}}}$. Similarly, compared to intersession CoV, intersubject CoV contains additional intersubject physiologic differences. These contributions can be calculated as $\sqrt{\mathrm{CoV}^2_{\mathrm{intersubject}} - \mathrm{CoV}^2_{\mathrm{intersession}}}$.

Additionally, as CBF quantification involves manual ROI selection, inter-rater reliability of CBF measurement was evaluated by having two raters (PL and FX) analyze the same datasets independently and calculating the correlation of the CBF values.

Relationships between physiologic parameters were evaluated with Pearson correlation and mixed effect model. In all analyses, a $P < 0.05$ is considered statistically significant.

RESULTS

All subjects successfully completed all sessions. Representative PC and TRUST MR images are shown in Fig. 2c,e, respectively. Table 1 summarizes the average values and the intrasession, intersession, and intersubject CoV for Y_v, OEF, CBF, and $CMRO_2$. It can be seen that the intrasession CoV, which reflects the measurement noise, is less than 4% for all parameters, suggesting high reliability of the techniques used. Figure 3a,b show a Bland–Altman plot and a scatter plot, respectively, between two $CMRO_2$ measurements in the same session, again demonstrating a strong consistency across measurements ($r = 0.67$, $P < 0.001$).

Intersession CoV was higher than intrasession CoV (Table 1), as addition sources of variance are included. The subject repositioning and day-to-day physiologic fluctuations, as calculated by the root square difference between Intersubject CoV, were estimated to be 5.35% for $CMRO_2$ measurements.

Intersubject CoV was 8.8% for $CMRO_2$ measurements (Table 1). It is interesting to note that intersubject variations in CBF and OEF were much greater ($P < 0.001$) than that of their product, $CMRO_2$. This is because CBF and OEF covary across individuals, as can be seen in their scatter plot (Fig. 4, $P = 0.01$). That is, an individual with a higher CBF tends to have a lower OEF, thus their effects partly cancel out in the $CMRO_2$. In fact, the same statement can be made for measurements across sessions (see dots with the same colors in Fig. 4, mixed effect model $P = 0.002$). That is, if a subject shows a higher CBF in a session, his OEF in this session will tend to be lower.

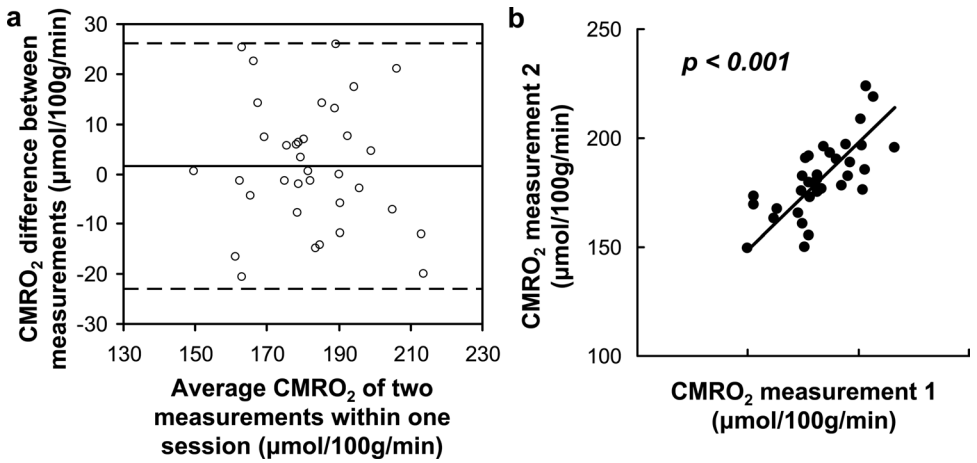

FIG. 3. Intrasession reproducibility of the $CMRO_2$ measurements. **a**: Bland–Altman plot comparing two $CMRO_2$ measurements obtained within one session. The solid line indicates the mean difference between two measurements. The dashed lines indicate the 95% confidence interval. **b**: Scatter plot of the two $CMRO_2$ measurements. Each dot represents data from one session of one subject. The solid line indicates the linear regression curve ($r = 0.67$, $P < 0.0001$).

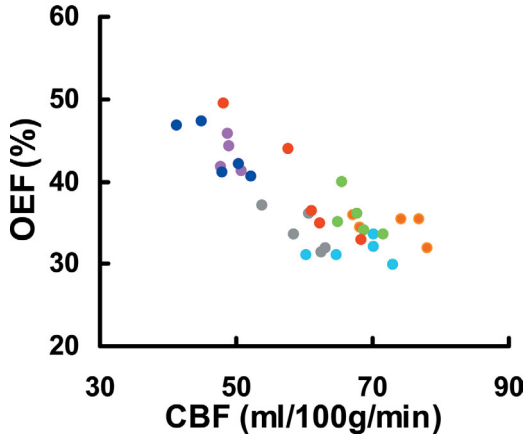

FIG. 4. Scatter plot of CBF and OEF measurements across subjects and across sessions. Each dot represents data from one session of one subject. Different sessions from one subject are shown in the same color. CBF and OEF are correlated across sessions ($P = 0.002$ from mixed effect model analysis) and across subjects ($P = 0.01$ from Pearson correlation). [Color figure can be viewed in the online issue, which is available at wileyonlinelibrary.com.]

For CBF processing which involves manual ROI drawing, we observed a high inter-rater reliability of $r = 0.997$ and $P < 0.0001$ (fitting line $y = 1.002\times$).

DISCUSSION

The $CMRO_2$ method under investigation, originally proposed by Xu et al. (21), has great potentials in understanding brain physiology and brain diseases (4,5,35–37). Compared to the few existing $CMRO_2$ methods including ^{15}O PET (12–15), ^{13}C NMR (19), and ^{17}O NMR (16), this method has the advantages of being noninvasive (no exogenous agent needed), rapid (<5 min in scan time), and can be implemented on a standard clinical scanner. Critical but missing steps are the establishment of a standard acquisition procedure and a thorough investigation of test–retest reproducibility. The present study intends to fill these gaps. Here, we provide step-by-step instructions on the orders of the necessary scans with details on slice positioning. The performance of this procedure was tested extensively from the data in the present study as well as other ongoing studies in our laboratory. While all previous test–retest studies on $CMRO_2$ have only attempted two sessions (12,13,16,27), we conducted a five-session reproducibility evaluation and showed that global $CMRO_2$ measured with this method has an intrasession, intersession, and intersubject CoV of 4, 7, and 9%, respectively. These data provide an important reference for future studies when deciding whether this method can be applied or when conducting power calculations.

The intrasession CoV of the present technique (Table 1) was slightly lower than those reported for ^{15}O PET, which was found to be 5.7 ± 4.4%, 8.4 ± 7.6%, and 5.3 ± 3.9% for OEF, CBF and $CMRO_2$, respectively (13). For intersession CoV, the values obtained in this study was comparable to the PET reports, which were 9.3, 8.8, and 5.3% for OEF, CBF, and $CMRO_2$, respectively (12). The intersubject CoV in the present study is also in good agreement with that in the PET studies, which ranged from 7.1 to 12.8% (12,13). Compared to CBF measurements with arterial-spin-labeling techniques, which showed an intrasession CoV of 3.5–7.5% and an intersession CoV of 8.5–16.6% (44), the PC MRI technique used in the present study showed a smaller variation, presumably because arterial-spin-labeling MRI contains a few confounding factors associated with labeling efficiency, arterial transit time, and T_1 relaxation (45,46). It should be mentioned that several other noninvasive $CMRO_2$ methods have been proposed recently. These methods were based on susceptibility effect in extravascular tissue (20,29), phase angle in intravascular blood signal (30), and T_2 value of regional blood signal (47). A full assessment of test–retest reproducibility of these methods has not been reported and should be investigated in future studies.

Compared to the procedure used in the original report of this technique (21), the proposed protocol have made the following changes/improvements. For the estimation of Y_v, Xu et al. have recently proposed a modified TRUST sequence in which a nonselective saturation RF pulse was applied immediately after image acquisition to reset the magnetizations of all spins (38). When combined with an optimal TR and TE, this sequence was found to reduce the scan duration by 63% while maintaining estimating accuracy and precision (38). This improvement in TRUST technique has been adopted in this study. For PC MRI, the previous report applied the imaging slice at the level of cervical spinal cord 3 (C3), where all four arteries (left/right internal carotid artery, left/right VA) were parallel to each other. While this position allows the arteries to be "capture" in one PC scan, it has three pitfalls. First, any arterial branching (or even merging) between this location and the foramen magnum, where the arteries enter the skull, could result in bias in CBF estimation. Second, the level of C3 is more distant from the iso-center of the magnet, thus the actual gradient strength experienced by the blood spins may be lower than nominal values, resulting in underestimation in flow velocity. Finally, in some individuals, the common carotid artery has not branched at this level, thus the estimated flow may include both internal and external carotids. Therefore, in this study, we acquired PC MRI at a higher location immediately adjacent to foramen magnum using four separate scans. The additional time needed for extra PC scans was offset by the time saved from the TRUST scan. Thus, the total time was still within 5 min.

We observed that CBF and OEF covaried across sessions and across subjects, and as a result, the variations in $CMRO_2$, the product of CBF and OEF were actually smaller than those of the individual factors. That is, although vascular parameters (blood flow and blood oxygenation) show large intersubject variations due to numerous physiologic reasons (e.g., breathing pattern, blood pressure, consumption of caffeine), the brain's metabolic rate does not show much variability across days or across individuals of similar age, making this parameter an excellent biomarker for studies of diseased conditions.

Compared to the calibrated fMRI technique, the $CMRO_2$ method used in this study does not require the

use of inhalation tasks such as hypercapnia or hyperoxia (24–26,28) and the measurement duration is relatively short. In fact, the proposed method may be applied to physiologic challenges to test certain assumptions made in the calibrated fMRI method (e.g., hypercapnia and hyperoxia do not alter $CMRO_2$) (35,36). On the other hand, the advantage of calibrated fMRI is that this technique provides a potential to map $CMRO_2$ on a region-by-region basis (28).

The main limitation of the present $CMRO_2$ technique is its lack of spatial resolution. The evaluations of Y_v, CBF, and $CMRO_2$ were all based on global measures. As this technique cannot provide regional $CMRO_2$ information, this technique will have limited utility in brain diseases with focal or inhomogeneous metabolic changes, such as acute stroke and brain tumor, unless the lesion regions cover the majority of the brain. However, global $CMRO_2$ may find applications in certain clinical scenarios, especially given that the technique can be completed within 5 min with a small CoV of 4% using completely noninvasive procedures on a standard 3T system. We have previously demonstrated the utility of this technique in cognitive aging (4), multiple sclerosis (5), and CO_2 modulation of brain metabolism (35). This technique can also be applied to other pathological conditions. In particular, the present technique may be of great benefit in studies of brain development in children including neonates, in whom the use of radioactively labeled tracers may not be justifiable.

A physiologic confound of the present technique is hematocrit. The hematocrit level may affect the estimated $CMRO_2$ value by two means. One is that the relationship between blood T_2 and oxygenation is dependent on hematocrit and thus, for the same measured T_2, the actual oxygenation could be slightly different for different hematocrit. A second effect is that the value of C_a in Eq. 1 is expected to be proportional to hematocrit because the oxygen carrying capacity will be greater if there is more hemoglobin in the blood. Fortunately, these two confounding effects of hematocrit have opposite consequences on $CMRO_2$; thus, they partially cancel out. Our earlier simulation study showed that, within normal hematocrit range of 0.38–0.50, the bias in the estimated $CMRO_2$ was −5.6 to 7.1% of the true value (21). However, for conditions where hematocrit may be substantially out of normal range (e.g., anemia), a blood sample should be obtained and a hematocrit-specific blood calibration curve (40) and C_a should be used in the calculation of $CMRO_2$. Similarly, in conditions where red blood cell or hemoglobin is different (e.g., sickle cell disease (48), fetal hemoglobin in neonate applications (49)), new blood calibration curves should be obtained for accurate estimation of $CMRO_2$.

CONCLUSIONS

Intrasession and intersession variability of the proposed $CMRO_2$ procedure is comparable or slightly smaller than that using ^{15}O PET. Intersubject variations in $CMRO_2$ were found to be smaller than that of the vascular parameters, CBF and OEF. Its simplicity and reliability features may afford this technique great potential for immediate clinical applications.

REFERENCES

1. Magistretti PJ, Pellerin L. Cellular mechanisms of brain energy metabolism and their relevance to functional brain imaging. Philos Trans R Soc Lond B Biol Sci 1999;354:1155–1163.
2. Buckner RL, Snyder AZ, Shannon BJ, LaRossa G, Sachs R, Fotenos AF, Sheline YI, Klunk WE, Mathis CA, Morris JC, Mintun MA. Molecular, structural, and functional characterization of Alzheimer's disease: evidence for a relationship between default activity, amyloid, and memory. J Neurosci 2005;25:7709–7717.
3. Ogawa M, Fukuyama H, Ouchi Y, Yamauchi H, Kimura J. Altered energy metabolism in Alzheimer's disease. J Neurol Sci 1996;139: 78–82.
4. Lu H, Xu F, Rodrigue KM, Kennedy KM, Cheng Y, Flicker B, Hebrank AC, Uh J, Park DC. Alterations in cerebral metabolic rate and blood supply across the adult lifespan. Cereb Cortex 2011;21: 1426–1434.
5. Ge Y, Zhang Z, Lu H, Tang L, Jaggi H, Herbert J, Babb JS, Rusinek H, Grossman RI. Characterizing brain oxygen metabolism in patients with multiple sclerosis with T2-relaxation-under-spin-tagging MRI. J Cereb Blood Flow Metab 2012;32:403–412.
6. Sun X, Tanaka M, Kondo S, Okamoto K, Hirai S. Clinical significance of reduced cerebral metabolism in multiple sclerosis: a combined PET and MRI study. Ann Nucl Med 1998;12:89–94.
7. Borghammer P, Vafaee M, Ostergaard K, Rodell A, Bailey C, Cumming P. Effect of memantine on CBF and CMRO2 in patients with early Parkinson's disease. Acta Neurol Scand 2008;117:317–323.
8. Sieber FE, Brown PR, Wu Y, Koehler RC, Traystman RJ. Cerebral blood flow and metabolism in dogs with chronic diabetes. Anesthesiology 1993;79:1013–1021.
9. Uchino K, Lin R, Zaidi SF, Kuwabara H, Sashin D, Bircher N, Chang YF, Hammer MD, Reddy V, Jovin TG, Vora N, Jumaa M, Massaro L, Billigen J, Boada F, Yonas H, Nemoto EM. Increased cerebral oxygen metabolism and ischemic stress in subjects with metabolic syndrome-associated risk factors: preliminary observations. Transl Stroke Res 2010;1:178–183.
10. Glenn TC, Kelly DF, Boscardin WJ, McArthur DL, Vespa P, Oertel M, Hovda DA, Bergsneider M, Hillered L, Martin NA. Energy dysfunction as a predictor of outcome after moderate or severe head injury: indices of oxygen, glucose, and lactate metabolism. J Cereb Blood Flow Metab 2003;23:1239–1250.
11. Walter C, Hertel F, Naumann E, Morsdorf M. Alteration of cerebral perfusion in patients with idiopathic normal pressure hydrocephalus measured by 3D perfusion weighted magnetic resonance imaging. J Neurol 2005;252:1465–1471.
12. Bremmer JP, van Berckel BN, Persoon S, Kappelle LJ, Lammertsma AA, Kloet R, Luurtsema G, Rijbroek A, Klijn CJ, Boellaard R. Day-to-day test-retest variability of CBF, CMRO2, and OEF measurements using dynamic 15O PET studies. Mol Imaging Biol 2011;13:759–768.
13. Coles JP, Fryer TD, Bradley PG, Nortje J, Smielewski P, Rice K, Clark JC, Pickard JD, Menon DK. Intersubject variability and reproducibility of 15O PET studies. J Cereb Blood Flow Metab 2006;26:48–57.
14. Fox PT, Raichle ME. Focal physiological uncoupling of cerebral blood flow and oxidative metabolism during somatosensory stimulation in human subjects. Proc Natl Acad Sci USA 1986;83:1140–1144.
15. Mintun MA, Raichle ME, Martin WR, Herscovitch P. Brain oxygen utilization measured with O-15 radiotracers and positron emission tomography. J Nucl Med 1984;25:177–187.
16. Zhu XH, Zhang Y, Tian RX, Lei H, Zhang N, Zhang X, Merkle H, Ugurbil K, Chen W. Development of (17)O NMR approach for fast imaging of cerebral metabolic rate of oxygen in rat brain at high field. Proc Natl Acad Sci USA 2002;99:13194–13199.
17. Kety SS, Schmidt CF. The effects of altered arterial tensions of carbon dioxide and oxygen on cerebral blood flow and cerebral oxygen consumption of normal young men. J Clin Invest 1948;27:484–492.
18. Taudorf S, Berg RM, Bailey DM, Moller K. Cerebral blood flow and oxygen metabolism measured with the Kety-Schmidt method using nitrous oxide. Acta Anaesthesiol Scand 2009;53:159–167.
19. Hyder F, Chase JR, Behar KL, Mason GF, Siddeek M, Rothman DL, Shulman RG. Increased tricarboxylic acid cycle flux in rat brain during forepaw stimulation detected with 1H[13C]NMR. Proc Natl Acad Sci USA 1996;93:7612–7617.

20. An H, Lin W, Celik A, Lee YZ. Quantitative measurements of cerebral metabolic rate of oxygen utilization using MRI: a volunteer study. NMR Biomed 2001;14:441–447.
21. Xu F, Ge Y, Lu H. Noninvasive quantification of whole-brain cerebral metabolic rate of oxygen (CMRO2) by MRI. Magn Reson Med 2009; 62:141–148.
22. Chen JJ, Pike GB. Global cerebral oxidative metabolism during hypercapnia and hypocapnia in humans: implications for BOLD fMRI. J Cereb Blood Flow Metab 2010;30:1094–1099.
23. Elwell CE, Henty JR, Leung TS, Austin T, Meek JH, Delpy DT, Wyatt JS. Measurement of CMRO2 in neonates undergoing intensive care using near infrared spectroscopy. Adv Exp Med Biol 2005;566: 263–268.
24. Davis TL, Kwong KK, Weisskoff RM, Rosen BR. Calibrated functional MRI: mapping the dynamics of oxidative metabolism. Proc Natl Acad Sci USA 1998;95:1834–1839.
25. Hoge RD, Atkinson J, Gill B, Crelier GR, Marrett S, Pike GB. Investigation of BOLD signal dependence on cerebral blood flow and oxygen consumption: the deoxyhemoglobin dilution model. Magn Reson Med 1999;42:849–863.
26. Chiarelli PA, Bulte DP, Gallichan D, Piechnik SK, Wise R, Jezzard P. Flow-metabolism coupling in human visual, motor, and supplementary motor areas assessed by magnetic resonance imaging. Magn Reson Med 2007;57:538–547.
27. Leontiev O, Buxton RB. Reproducibility of BOLD, perfusion, and CMRO2 measurements with calibrated-BOLD fMRI. Neuroimage 2007;35:175–184.
28. Gauthier CJ, Hoge RD. Magnetic resonance imaging of resting OEF and CMRO(2) using a generalized calibration model for hypercapnia and hyperoxia. Neuroimage 2012;60:1212–1225.
29. He X, Yablonskiy DA. Quantitative BOLD: mapping of human cerebral deoxygenated blood volume and oxygen extraction fraction: default state. Magn Reson Med 2007;57:115–126.
30. Jain V, Langham MC, Wehrli FW. MRI estimation of global brain oxygen consumption rate. J Cereb Blood Flow Metab 2010;30:1598–1607.
31. Brown DW, Hadway J, Lee TY. Near-infrared spectroscopy measurement of oxygen extraction fraction and cerebral metabolic rate of oxygen in newborn piglets. Pediatr Res 2003;54:861–867.
32. Tichauer KM, Elliott JT, Hadway JA, Lee DS, Lee TY, St Lawrence K. Using near-infrared spectroscopy to measure cerebral metabolic rate of oxygen under multiple levels of arterial oxygenation in piglets. J Appl Physiol 2010;109:878–885.
33. Haccke EM, Brown RW, Thompson MR, Venkatesan R. MR Angiography and flow quantification. magnetic resonance imaging: physical principles and sequence design. New York: Wiley-Liss;1999.
34. Lu H, Ge Y. Quantitative evaluation of oxygenation in venous vessels using T_2-relaxation-under-spin-tagging MRI. Magn Reson Med 2008; 60:357–363.
35. Xu F, Uh J, Brier MR, Hart J Jr, Yezhuvath US, Gu H, Yang Y, Lu H. The influence of carbon dioxide on brain activity and metabolism in conscious humans. J Cereb Blood Flow Metab 2011;31:58–67.
36. Xu F, Liu P, Lu H. Effect of graded O2 challenge on vascular and metabolic parameters. In Proceedings of the 19th Annual Meeting of ISMRM, Montreal, Canada, 2011. p. 253.
37. Xu F, Liu P, Lu H. Acute and chronic effects of glucose on brain metabolism: findings from healthy subjects and diseased conditions. In: Proceedings of the 20th Annual Meeting of ISMRM. Melbourne, Australia; 2012. p 2915.
38. Xu F, Uh J, Liu P, Lu H. On improving the speed and reliability of T(2)-relaxation-under-spin-tagging (TRUST) MRI. Magn Reson Med 2012;68:198–204.
39. Guyton AC, Hall JE. Respiration. In: Guyton AC, Hall JE, editors. Textbook of medical physiology, 11th ed. Philadelphia: Saunders/ Elsevier; 2005.
40. Lu H, Xu F, Grgac K, Liu P, Qin Q, van Zijl P. Calibration and validation of TRUST MRI for the estimation of cerebral blood oxygenation. Magn Reson Med 2012;67:42–49.
41. Bakker CJ, Hoogeveen RM, Viergever MA. Construction of a protocol for measuring blood flow by two-dimensional phase-contrast MRA. J Magn Reson Imaging 1999;9:119–127.
42. Evans AJ, Iwai F, Grist TA, Sostman HD, Hedlund LW, Spritzer CE, Negro-Vilar R, Beam CA, Pelc NJ. Magnetic resonance imaging of blood flow with a phase subtraction technique. In vitro and in vivo validation. Invest Radiol 1993;28:109–115.
43. Zananiri FV, Jackson PC, Goddard PR, Davies ER, Wells PN. An evaluation of the accuracy of flow measurements using magnetic resonance imaging (MRI). J Med Eng Technol 1991;15:170–176.
44. Chen Y, Wang DJ, Detre JA. Test-retest reliability of arterial spin labeling with common labeling strategies. J Magn Reson Imaging 2011;33:940–949.
45. Golay X, Hendrikse J, Lim TC. Perfusion imaging using arterial spin labeling. Top Magn Reson Imaging 2004;15:10–27.
46. Yang Y, Engelien W, Xu S, Gu H, Silbersweig DA, Stern E. Transit time, trailing time, and cerebral blood flow during brain activation: measurement using multislice, pulsed spin-labeling perfusion imaging. Magn Reson Med 2000;44:680–685.
47. Bolar DS, Rosen BR, Sorensen AG, Adalsteinsson E. Quantitative Imaging of extraction of oxygen and TIssue consumption (QUIXOTIC) using venular-targeted velocity-selective spin labeling. Magn Reson Med 2011;66:1550–1562.
48. Serjeant GR, Serjeant BE. Sickle cell disease. Oxford: Oxford University Press; 2001.
49. Zijlstra WG, Buursma A, Meeuwsen-van der Roest WP. Absorption spectra of human fetal and adult oxyhemoglobin, de-oxyhemoglobin, carboxyhemoglobin, and methemoglobin. Clin Chem 1991;37: 1633–1638.